Anal. Chem. **2000,** *72,* 4796−4804

Articles

Optical Patternation: A Technique for Three-Dimensional Aerosol Diagnostics

John A. McLean, Michael G. Minnich, and Akbar Montaser*

Department of Chemistry, George Washington University, Washington, D.C. 20052

Jeff Su and Wing Lai

Aerometrics/TSI Incorporated, St. Paul, Minnesota 55164

A novel technique based on optical patternation is described for three-dimensional diagnostic studies of aerosols used in analytical spectroscopies. The aerosol is illuminated with a thin laser light sheet to capture images of the fluorescence and Lorenz−Mie light-scattering signals from the aerosol field with a charge-coupled detector. These measurements allow for the rapid and nonintrusive elucidation of two-dimensional spray structures, planar mass distributions, and spatial droplet size distributions. The ratio of the fluorescence image to the Lorenz−Mie image is then utilized to construct a spatially resolved map of the volume-to-surface area mean of the aerosol (Sauter mean diameter). Three-dimensional maps of spray structure, mass distribution, and droplet size distribution are obtained for the entire aerosol field by image stacking. The technique is applied to the measurement of the droplet size over the aerosol field at distances of 5−30 mm from the nebulizer tip where droplet sizes ranged from 6 to 12 μm for a direct injection high efficiency nebulizer used in inductively coupled plasma spectrometries.

Introduction of sample into plasmas plays a key role in the production of excited species and ions and the generation of interfering species, noise, and matrix effects in plasma spectrometries.[1−8] Nebulizer diagnostic techniques guide the design of sample introduction techniques, provide fundamental information for the quantitative assessment and prediction of the quality of the aerosol used in plasma spectrometries, and validate existing and emerging aerosol generation and plasma models.[2,9−16] In addition, nebulizer and aerosol diagnostic techniques have important applications in diverse fields such as environmental chemistry, aerosol drug delivery studies, development of new pharmaceutical products and various manufacturing processes, and investigation of fuel mixing in automobile engines and rockets.

Several approaches have been useful in investigating fundamental properties of nebulizers, aerosols, and plasmas in analytical spectrometries. For example, Lorenz−Mie scattering has been used to compare droplet size distributions produced by different nebulizers and to monitor aerosol desolvation and vaporization in argon inductively coupled plasma (Ar ICP) spectrometries.[17−20] Time-resolved optical emission has been applied to examine the influence of droplets on emission and ionization of analyte in the ICP, to track desolvated particles in the central channel of the plasma, to measure gas velocities, and to study space-charge effects in ICP mass spectrometry (ICPMS) and ICP atomic emission spectrometry (ICPAES).[21−32] High-speed photography,[3,33−35] laser Fraunhofer diffraction,[36−38] and phase-Doppler particle

* To whom correspondence should be addressed. Telephone: 202-994-6480. Fax: 202-994-2298. E-mail: montaser@gwis2.circ.gwu.edu.

(1) Montaser, A.; Minnich, M. G.; McLean, J. A.; Liu, H.; Caruso, J. A.; McLeod, C. W. Sample Introduction in ICPMS. In *Inductively Coupled Plasma Mass Spectrometry*; Montaser, A., Ed.; Wiley: New York, 1998.
(2) Montaser, A.; Minnich, M. G.; Liu, H.; Gustavsson, A. G. T.; Browner, R. F. Fundamental Aspects of Sample Introduction in ICP Spectrometry. In *Inductively Coupled Plasma Mass Spectrometry*; Montaser, A., Ed.; Wiley: New York, 1998.
(3) McLean, J. A.; Minnich, M. G.; Iacone, L. A.; Liu, H.; Montaser, A. *J. Anal. At. Spectrom.* **1998**, *13*, 829−842.
(4) Greenfield, S.; Montaser, A. Common RF Generators, Torches, and Sample Introduction Systems. In *Inductively Coupled Plasmas in Analytical Atomic Spectrometry*, 2nd ed.; Montaser, A., Ed.; Wiley-VCH: New York, 1992.
(5) Gustavsson, A. G. T. Liquid Sample Introduction into Plasmas. In *Inductively Coupled Plasmas in Analytical Atomic Spectrometry*, 2nd ed.; Montaser, A., Ed.; Wiley-VCH: New York, 1992.
(6) Sharp, B. L. *J. Anal. At. Spectrom.* **1988**, *3*, 613−652.
(7) Sharp, B. L. *J. Anal. At. Spectrom.* **1988**, *3*, 939−963.
(8) Browner, R. F. Fundamental Aspects of Aerosol Generation and Transport. In *Inductively Coupled Plasma Emission Spectroscopy, Part II*; Boumans, P. W. J. M., Ed.; Wiley: New York, 1987.
(9) Horner, J. A.; Hieftje, G. M. *Spectrochim. Acta* **1998**, *53B*, 1235−1259.
(10) Cave, M. *J. Anal. At. Spectrom.* **1998**, *13*, 125−129.
(11) Cai, M.; Haydar, D. A.; Montaser, A.; Mostaghimi, J. *Spectrochim. Acta* **1997**, *52B*, 369−386.
(12) Canals, A.; Hernandis, V.; Browner, R. F. *J. Anal. At. Spectrom.* **1990**, *5*, 61−66.
(13) Gustavsson, A. G. T. *Anal. Chem.* **1984**, *56*, 815−817; **1983**, *55*, 94−98.
(14) Benson, C. M.; Gimelshein, S. F.; Levin, D. A.; Montaser, A. Simulation of Droplet-Gas Interactions in an Inductively Coupled Plasma Using the Direct Simulation Monte Carlo Method. American Institute of Aeronautics and Astronautics 34th Thermophysics Conference, Denver, CO, June 19−22, 2000; Paper A1AA 2000-2431.
(15) Browner, R. F.; Boorn, A. W.; Smith, D. D. *Anal. Chem.* **1982**, *54*, 1411−1419.
(16) Nukiyama, S.; Tanasawa, Y. *Experiments on the Atomization of Liquids in an Air Stream*; Hope, E., transl.; Defense Research Board, Department of National Defense: Ottawa, Canada, 1950.
(17) Olsen, S. D.; Strasheim, A. *Spectrochim. Acta* **1983**, *38B*, 973−975.
(18) Clifford, R. H.; Montaser, A.; Sinex, S. A.; Capar, S. G. *Anal. Chem.* **1989**, *61*, 2777−2784.
(19) Wiederin, D. R.; Houk, R. S. *Appl. Spectrosc.* **1991**, *45*, 1408−1412.
(20) Monnig, C. A.; Koirtyohann, S. R. *Anal. Chem.* **1985**, *57*, 2533−2536.
(21) Cicerone, M. T.; Farnsworth, P. B. *Spectrochim. Acta* **1989**, *44B*, 897−907.

10.1021/ac000239y CCC: $19.00
Published on Web 08/30/2000

Table 1. Optical Methods Involving Single-Particle or Ensemble Light Scattering and the Main Aerosol Parameters Measured

methods	main aerosol parameters measured
single-particle techniques	
phase-Doppler particle anal.	particle size (spherical) particle velocity droplet number density volume flux
particle imaging velocimetry	particle velocity
laser-Doppler velocimetry	particle velocity
rainbow refractometry	particle temperature
aerodynamic particle sizer	particle size (spherical or nonspherical)
ratiometric particle anal.	particle size (spherical or nonspherical)
high-speed photography	particle size (spherical or nonspherical) particle velocity
particle ensemble techniques	
optical patternation	spatial spray structure spatial mass distribution spatial droplet size distribution
particle imaging velocimetry	particle velocity
laser Fraunhofer diffraction	droplet size distribution
planar laser-induced fluorescence	spatial mass distribution
high-speed photography	spray structure particle size nozzle tip velocities

analysis[3,39−42] have also been used to measure aerosol parameters and to elucidate fundamental sample introduction-related processes in plasmas.

In general, optical techniques for aerosol diagnostics have largely replaced mechanical means, because they are nonintrusive.[2,3,43] These techniques (Table 1) can be divided into two broad categories depending on whether single particles or particle ensembles are measured. In large part, different aerosol diagnostic techniques present complementary information based on the fundamental principles used. For example, phase-Doppler particle analysis provides droplet size and velocity information at a single point in space, while the Fraunhofer diffraction technique offers droplet size information over an integrated volume (Table 1). To measure spatially resolved droplet size distributions throughout the entire spray by a point measurement technique such as a phase-Doppler particle analyzer, the aerosol field must be probed sequentially and is not applicable when temporal resolution over the entire aerosol field is required. Alternatively, Abel inversion can be used to convert ensemble line-of-sight measurements to spatially resolved results. The Abel inversion technique is also difficult to implement and is prone to error in the central regions of the spray field. An ideal technique would offer an instantaneous snapshot of the entire three-dimensional droplet field for subsequent analysis. Holographic techniques provide the depth of field that is necessary for obtaining three-dimensional droplet field images, but they are limited to applications where the droplet diameter is greater than 15 μm.[44] Unfortunately, this diameter is larger than the droplet diameter that is most useful in plasma spectrometries (<8−10 μm).

This report describes the measurement principles behind a novel aerosol diagnostic technique known as optical patternation. The approach provides rapid and nonintrusive, spatially resolved spray structures, mass distributions, and particle size distributions in two dimensions. Three-dimensional (3D) maps of spray structure, mass distribution, and droplet size distribution are then constructed for the entire aerosol field by using image stacking. We discuss the utility of the technique in the diagnostic study of aerosols used for sample introduction in atomic spectrometries. The technique is applied to the 3D characterization of the primary aerosol produced by a direct injection high efficiency nebulizer (DIHEN).[3,45−47] The implications and importance of these results for sample introduction in ICP spectrometries are addressed.

Principles of Optical Patternation. In optical patternation,[3,48−54] a laser light sheet is formed to illuminate a slice through the sample aerosol. The fluorescence and light-scattering images are then captured with a camera such as a charge-coupled device

(22) Olesik, J. W.; Smith, L. J.; Williamsen, E. J. *Anal. Chem.* **1989**, *61*, 2002−2008.
(23) Olesik, J. W.; Williamsen, E. J. *Appl. Spectrosc.* **1989**, *43*, 933−940.
(24) Olesik, J. W.; Fister, J. C., III *Spectrochim. Acta* **1991**, *46B*, 851−868.
(25) Fister, J. C., III; Olesik, J. W. *Spectrochim. Acta* **1991**, *46B*, 869−883.
(26) Hobbs, S. E.; Olesik, J. W. *Anal. Chem.* **1992**, *64*, 274−283.
(27) Hobbs, S. E.; Olesik, J. W. *Spectrochim. Acta* **1993**, *48B*, 817−833.
(28) Olesik, J. W. *Anal. Chem.* **1996**, *68*, 469A−474A.
(29) Dziewatkoski, M. P.; Daniels, L. B.; Olesik, J. W. *Anal. Chem.* **1996**, *68*, 1101−1109.
(30) Olesik, J. W.; Dziewatkoski, M. P. *J. Am. Soc. Mass Spectrom.* **1996**, *7*, 362−367.
(31) Olesik, J. W. *Appl. Spectrosc.* **1997**, *51*, 158A−175A.
(32) Olesik, J. W.; Kinzer, J. A.; McGowan, G. J. *Appl. Spectrosc.* **1997**, *51*, 607−616.
(33) Winge, R. K.; Eckels, D. E.; DeKalb, E. L.; Fassel, V. A. *J. Anal. At. Spectrom.* **1988**, *3*, 849−855.
(34) Winge, R. K.; Crain, J. S.; Houk, R. S. *J. Anal. At. Spectrom.* **1991**, *6*, 601−604.
(35) Houk, R. S.; Winge, R. K.; Chen, X. *J. Anal. At. Spectrom.* **1997**, *12*, 1139−1148.
(36) Mohamed, N.; Fry, R. C.; Wetzel, D. L. *Anal. Chem.* **1981**, *53*, 639−645.
(37) Canals, A.; Wagner, J.; Browner, R. F.; Hernandis, V. *Spectrochim. Acta* **1988**, *43B*, 1321−1335.
(38) Olesik, J. W.; Bates, L. C. *Spectrochim. Acta* **1995**, *50B*, 285−303.
(39) Clifford, R. H.; Ishii, I.; Montaser, A.; Meyer, G. A. *Anal. Chem.* **1990**, *62*, 390−394.
(40) Clifford, R. H.; Sohal, P.; Liu, H.; Montaser, A. *Spectrochim. Acta* **1992**, *47B*, 1107−1122.
(41) Shum, S. C. K.; Johnson, S. K.; Pang, H.-M.; Houk, R. S. *Appl. Spectrosc.* **1993**, *47*, 575−583.
(42) Liu, H.; Montaser, A. *Anal. Chem.* **1994**, *66*, 3233−3242.
(43) Bachalo, W. D. *Int. J. Multiphase Flow* **1994**, *20*, 261−295.
(44) Thompson, B. J. Droplet Characteristics with Conventional and Holographic Imaging Techniques. in *Liquid Particle Size Measurement Techniques*; Tishkoff, J. M., Ingebo, R. D., Kennedy, J. B., Eds.; ASTM Special Technical Publication 848; American Society for Testing and Materials: Philadelphia, PA, 1984; pp 111−122.
(45) McLean, J. A.; Zhang, H.; Montaser, A. *Anal. Chem.* **1998**, *70*, 1012−1020.
(46) Singh, J.; McLean, J. A.; Pritchard, D. E.; Montaser, A.; Patierno, S. R. *Toxicol. Sci.* **1998**, *46*, 260−265.
(47) Becker, J. S.; Dietze, H.-J.; McLean, J. A.; Montaser, A. *Anal. Chem.* **1999**, *71*, 3077−3084.
(48) Sankar, S. V.; Robart, D. M.; Bachalo, W. D. A Planar Droplet Sizing Technique for Spray Characterization. *9th Annual Conference on Liquid Atomization and Spray Systems*, San Francisco, CA, May 19−22, 1996.
(49) Sankar, S. V.; Maher, K. E.; Bachalo, W. D. Time-Resolved Measurement of Liquid Mass Distribution in a Fuel Injector Spray Using an Optical Patternator. *10th Annual Conference on Liquid Atomization and Spray Systems*, Ottawa, Canada, May 18−21, 1997.
(50) Sankar, S. V.; Maher, K. E.; Robart, D. M.; Bachalo, W. D. Spray Characterization Using A Planar Droplet Sizing Technique. *7th International Conference on Liquid Atomization and Spray Systems*, Seoul, Korea, August 18−22, 1997.
(51) Sallens, R.; Deljouravesh, R. Non-Orthogonal Optical Spray Pattern Analysis. *11th Annual Conference on Liquid Atomization and Spray Systems*, Sacramento, CA, May 19−22, 1998.
(52) Su, J.; Ginestet, J.; Rudoff, R. Quantitative Characterization of Transient Fuel Sprays Using PLIF Imaging. *ASME International Fluid Mechanics Conference*, Washington, DC, June 23, 1998.

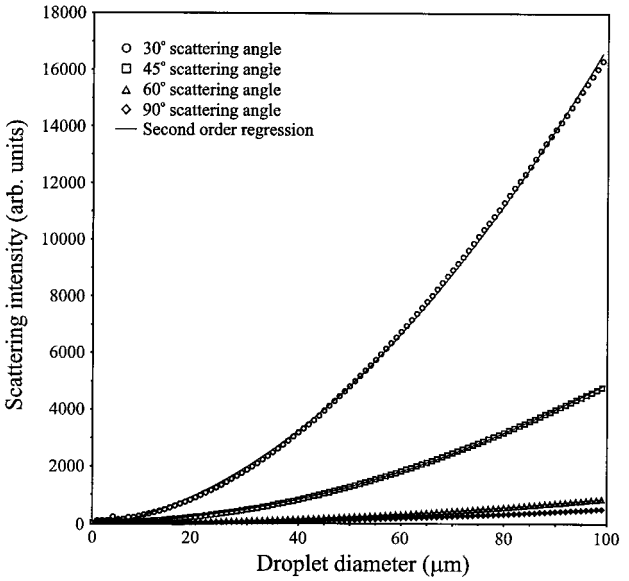

Figure 1. Computed Lorenz−Mie light scattering intensity as a function of droplet diameter for scattering angles of 30°, 45°, 60°, and 90°, respectively. All calculations were performed using Lorenz−Mie theory using a droplet refractive index of 1.334−0.04*i*. Solid lines represent a second-order regression on the calculated data ($N = 100$) for the particular scattering angle. In all cases, correlation coefficients are 0.9996 or better.

(CCD). The ratio of the fluorescence to Lorenz−Mie elastic light scattering is then used to construct maps of planar Sauter mean droplet diameter (D_{32}) distributions.

Optical patternation relies in part on Lorenz−Mie theory, which provides a mathematical solution to Maxwell's equations for the nonisotropic light scattering by homogeneous spherical particles at any location in space.[55,56] The scattering intensity depends on the wavelength, scattering angle, polarization of the incident light beam, refractive index, and particle size. When the imaginary component of the refractive index is small but nonzero, light scattering smoothly varies as the square of droplet diameter for different scattering angles.[50,53] The droplets absorb a small fraction of the incident light intensity which excites fluorescence in optical patternation.

Figure 1 shows the theoretical Lorenz−Mie scattering intensity calculated in this work for scattering angles of 30°, 45°, 60°, and 90° as a function of droplet diameter. The algorithms used for these calculations are presented elsewhere.[57] In these algorithms, the wavelength, scattering angle, polarization, refractive index at both the surface and core of the droplet, and particle size are considered. The wavelength of incident light was chosen to be 514.5 nm, corresponding to one of the most intense Ar^+ laser lines. The droplet index of refraction was 1.334−0.04*i*. Scattering angles of 30° and 90° were selected, because they closely approximate the oblique (32.5°) and orthogonal (90°) angles used to obtain aerosol images recorded in this work. A second-order polynomial regression fits the data, with a correlation coefficient of better than 0.9996 in all cases. Importantly, for any scattering angle, the relative Lorenz−Mie scattering intensity (I_e) is approximated by

$$I_e = kd^2 \tag{1}$$

where k is a scattering angle constant and d is the droplet diameter.[48] Provided an ensemble of droplets is measured in a two-dimensional plane, the spatial equation for elastic light-scattering intensity is described by

$$I_e(x, y) = I_i(x, y)\kappa \sum n_i(x, y)d_i^2(x, y) \tag{2}$$

Here, $I_e(x,y)$ is the spatial elastic scattering intensity, $I_i(x,y)$ is the intensity of the incident light source, κ is an elastic scattering constant, and n_i is the number of droplets of size class d_i for a particular (x,y) location. Because an ensemble of droplets is measured rather than individual droplets or particles, spatial distributions represent the integral moment of the respective distribution for the particular x,y location.

If the aerosol contains suitable fluorescing species or is doped with a fluorescent dye such as fluorescein or Rhodamine 6G, then the total fluorescence, an isotropic process, will depend on the incident excitation light intensity $I_i(x,y)$, the number of fluorescent species, the mass (or volume, d^3) of the droplets, and the concentration of fluorescent species in the vapor phase. Assuming negligible fluorescent species in the vapor phase, the spatial equation describing the fluorescent (I_f) light scattering is given by

$$I_f(x,y) = I_i(x,y)\phi \sum n_i(x, y)d_i^3(x, y) \tag{3}$$

where $I_f(x,y)$ is the spatial fluorescence intensity and ϕ is a fluorescence proportionality constant. A map proportional to the Sauter mean diameter (D_{32}) in two dimensions can be obtained by dividing the spatial fluorescent and elastic light scattering. In short, the ratio of eqs 3 to 2 yields the volume-to-surface area ratio of the sampled aerosol:

$$D_{32}(x, y) = \frac{\kappa}{\phi}\left(\frac{I_f(x, y)}{I_e(x, y)}\right) \tag{4}$$

Because ϕ and κ are constants, the intensity scale of the $I_f(x,y)/I_e(x,y)$ image is linearly proportional to $D_{32}(x, y)$ by a line of slope ϕ/κ.

EXPERIMENTAL SECTION

Aerosol Diagnostics by Optical Patternation. A schematic diagram of the optical patternator is presented in Figure 2 for both orthogonal and oblique image acquisition. In principle, this instrument is similar to the instrument assembled in our original optical patternation studies of two micronebulizers.[3,54] A laser light sheet was generated to produce Lorenz−Mie scattering and to excite fluorescence of the aerosol by passing the 488-nm continuous-wave output of a 7-W argon ion laser (model Innova 70, Coherent, Inc., Santa Clara, CA) through a cylindrical divergence

(53) Su, J.; Ginestet, J.; Rudoff, R. Quantitative Characterization of Liquid Sprays Using Phase Doppler Particle Analyzer and Optical Patternator. *1998 VSJ-SPIE International Conference on Optical Technology and Image Processing in Fluid, Thermal, and Combustion Flow*, Yokohama, Japan, December 6−9, 1998.
(54) McLean, J. A.; Huff, R. A.; Montaser, A. *Appl. Spectrosc.* **1999**, *53*, 1331−1340.
(55) Mie, G. *Ann. Phys.* **1908**, *25*, 377−445.
(56) Van de Hulst, H. C. Rigorous Scattering Theory for Spheres of Arbitrary Size (Mie Theory). In *Light Scattering by Small Particles*; Van de Hulst, H. C., Ed.; Wiley: New York, 1957.

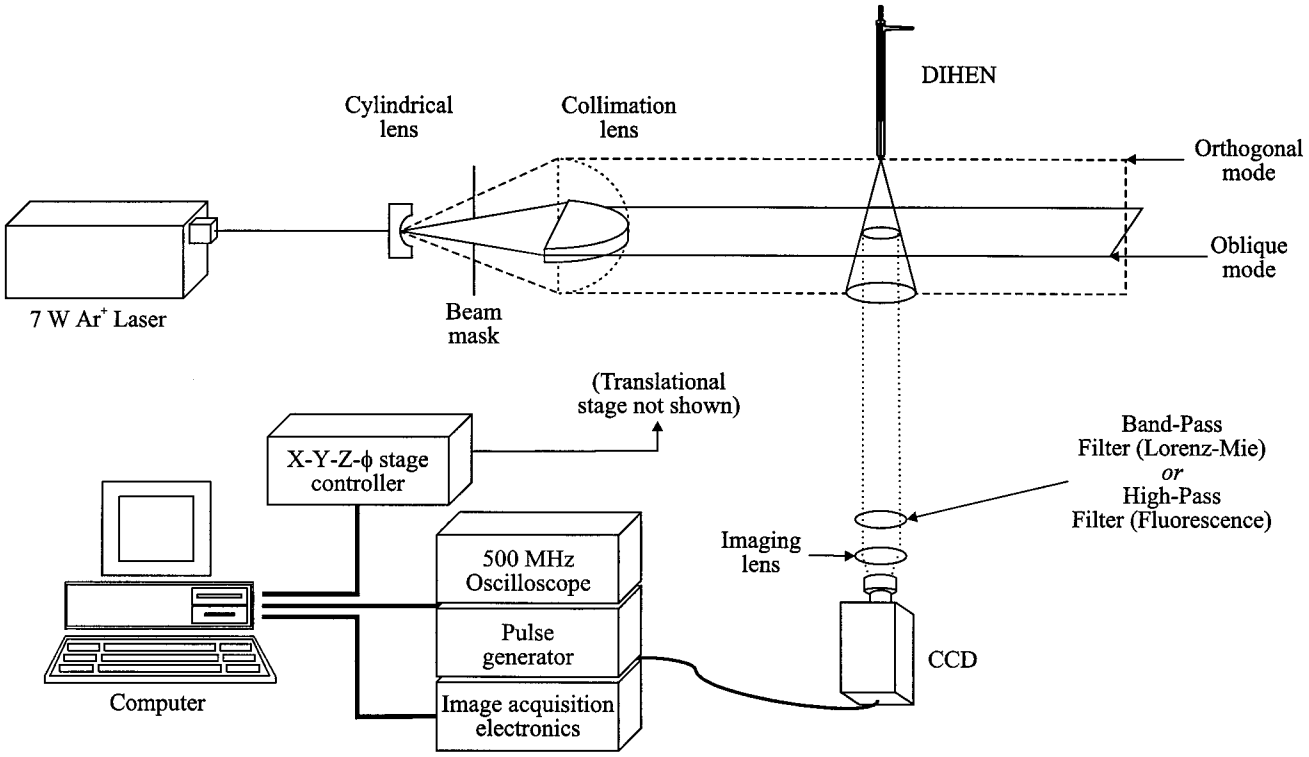

Figure 2. Schematic diagram of the optical patternator used in this work in either the orthogonal or oblique mode by orienting the cylindrical lens and collimation lens so that the light sheet was either parallel or perpendicular to the direction of spray propogation, respectively.

lens, a rectangular beam mask, and then a parabolic collimator. This arrangement resulted in a light sheet of 2-mm thickness and 124-mm width. Laser fluence was maintained at 2.09 W, which provided a power density of ~840 mW/cm^2. Images of the scattered and fluorescent light were registered using a 576 × 384 square pixel intensified CCD array (model ITE-576, Princeton Instruments, Inc., Trenton, NJ) with 16-bit dynamic range. Exposure times on the CCD array and gain for the microchannel plate were controlled by a pulse generator (model PG-10, Princeton Instruments, Inc.). Actual exposure times were recorded using a 500-MHz digital oscilloscope (model TDS 744A, Tektronix, Portland, OR). For Lorenz−Mie and fluorescence measurements, a 488- (10-nm band-pass) or a 515-nm high-pass cutoff filter (Andover Corp., Salem, NH) was alternately placed in front of the CCD array, respectively. To ensure that the Lorenz−Mie and fluorescent images fell within the dynamic range of the camera and near one another in relative intensity, various metallic neutral density filters (Andover Corp.) were used. For orthogonal images, the light sheet was oriented parallel to the axis of spray propogation. For oblique images, the light sheet was oriented perpendicular to the axis of the nebulizer. Image acquisition and image corrections (see below) were performed by the instrumental software (Optical Patternator version 1.1, Aerometrics/TSI Inc., St. Paul, MN) written to operate in the LabView 4.1 environment (National Instruments, Austin, TX). Images were then imported into a commercial graphics software package (CorelDraw 8, Corel Corp., Ottawa, Canada) for stacking and to add perspective to images as noted in the text.

Direct Injection High Efficiency Nebulizer. The analytical aerosol was generated using a DIHEN (model DIHEN-170-AA, J E Meinhard Associates, Inc., Santa Ana, CA) that has been described for use in ICPMS.[45−47] A test solution of water doped with fluorescein was delivered to the DIHEN at a solution flow rate of 85 μL/min via a syringe pump (model 341B, Sage Instruments, Boston, MA). The injector gas flow rate was maintained at 0.25 L/min by a mass flow controller (model 8200, Matheson Gas Products, East Rutherford, NJ). The DIHEN was translated relative to the light sheet via a $X-Y-Z-\phi$ translational stage (model Unidex 12, Aerotech, Inc., Pittsburgh, PA) operated by the patternator software. The stage could be moved with a precision of 0.001 in..

Aerosol Diagnostics by Phase-Doppler Particle Analysis. To convert the scaled ratio images into images of spatial Sauter mean diameter, a 2D phase-Doppler particle analyzer (PDPA, Aerometrics/TSI Inc.) was used.[45,54] For these studies, it was assumed that the spray was steady state and stable; thus, PDPA measurements and optical patternation measurements were not conducted simultaneously. The photomultiplier tubes were operated at −501 V. The receiver optics were held at a forward scattering angle of 30° with respect to the transmitter, and the aerosol was probed with the nebulizer oriented vertically downward as used for optical patternation experiments. The scattering signal produced from nonspherical particles, or multiple droplets in the probe volume, was rejected by comparing the phase shift measured across differently spaced detectors. If the phase shift measured varied by greater than 6%, the measurement was discarded by the signal-processing unit. For these measurements, the DIHEN was mounted on a manual $X-Y-Z$ stage and was moved with respect to the sampling volume of the PDPA. To calibrate the scaled ratio images obtained with the optical patternator, the PDPA was rastered through the plane corresponding to the optical patternator image. Five PDPA measurements (~50 000 droplets) at each point were obtained and then averaged to prepare a calibration curve converting the scaled ratio images into images of D_{32}. Two distinct aerosol regions (e.g.,

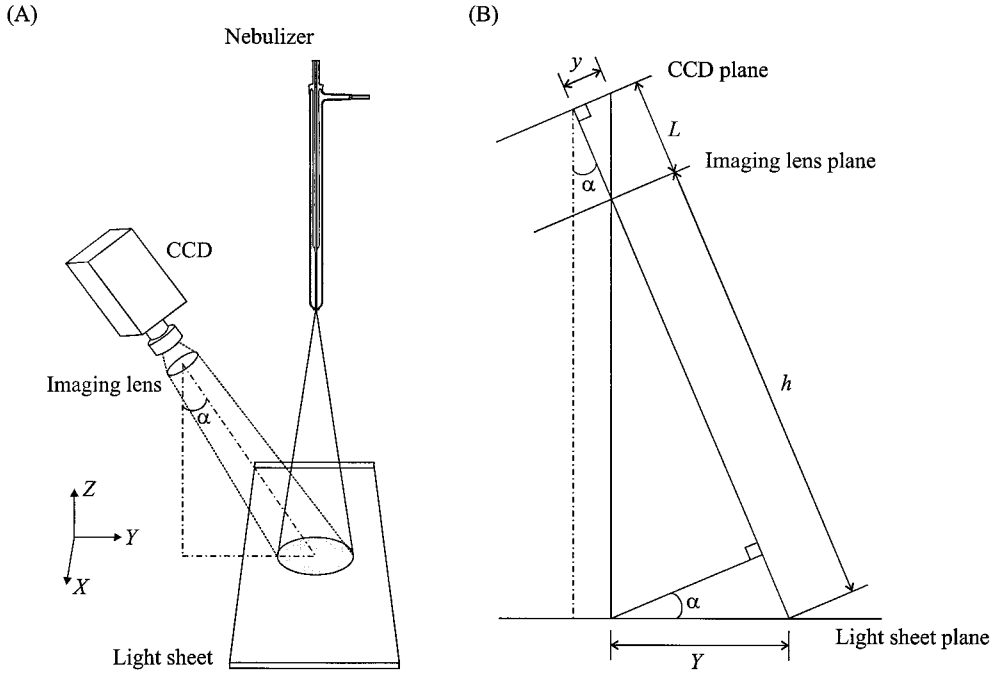

Figure 3. (A) Experimental arrangement for oblique-mode viewing using optical patternation and (B) trigonometric relationships used to correct for oblique-mode perspective distortion (Adapted from ref 58).

center and fringe regions) representing two diverse colors in Figure 4D were used to establish the calibration curve.

RESULTS AND DISCUSSION

In our previous work, we described optical patternation for the investigation of spray structures produced by two different nebulizers used in ICP spectrometries.[3,54] For the present studies, fluorescence images were also acquired to provide spatial mass distributions and planar droplet size distributions. However, image-processing steps, as discussed below, are necessary to acquire quantitative images in optical patternation.

Optical Patternator Image Processing. Three images are necessary to convert raw pixel intensities into spatially quantitative intensity maps for both Lorenz−Mie and fluorescent operation. A dark image ($I_{dark}(x, y)$) is first acquired to account for the dark current of the CCD array and the microchannel plate for a given gain. To account for variations in the response function of individual pixel elements, a uniform white light source is then used to illuminate the array ($I_{white}(x, y)$). Finally, one must also account for inhomogeneities in the laser light sheet used for aerosol illumination and fluorescence excitation. The homogeneity of the light sheet is controlled by the quality of the optical components used. To correct for these inhomogeneities, a rectangular plastic bar doped with a uniform concentration of fluoresein is placed directly in the path of the light sheet and an image of the light sheet profile ($I_{lsp}(y)$) is acquired over a few pixel columns (1−5). The average intensity values for the columns of pixel elements illuminated by the fluoresein bar is then propagated across the respective rows of the CCD array to give an image $I_{lsp}(x,y)$. Thus, for a fixed set of camera conditions (prime denotes that microchannel plate gain and/or camera exposure time may be different than that used for the raw image), the corrected image ($I_c(x, y)$, either Lorenz−Mie or fluorescence) is given by

$$I_c(x, y) = \left(\frac{[I_{raw}(x, y) - I_{dark}(x, y)]}{[I_{white}(x, y) - I_{dark}(x, y)]} \Big/ \frac{[I'_{lsp}(x, y) - I'_{dark}(x, y)]}{[I'_{white}(x, y) - I'_{dark}(x, y)]} \right) \quad (5)$$

Image fluctuations due to variations in the laser output power is a potential concern, but such variations may be largely minimized in some applications by time averaging. Additionally, because of the random position of an ensemble of droplets in the plane of the light sheet, the light-scattering signals or fluorescence signals lack coherence from droplets in the aerosol field and should not produce an interference pattern.[53]

Oblique-Viewing Image Foreshortening. For oblique-mode operation, one further correction is necessary to account for the perspective distortion inherent in the viewing angle of the camera. In this mode, the CCD plane does not reside in a plane parallel to the light sheet (Figure 3A). The illuminated circular slice of the aerosol, in the raw image, appears as an oval due to the perspective foreshortening. Here the size of a perspective projected object in the imaging plane varies inversely with the distance of the object in the projection plane. In the computer graphics community, three-dimensional perspective transformations are performed using a homogeneous matrix approach. A straightforward algebraic expression relates the image and the object based on geometrical optics.[58] The trigonometric relation between the object and the CCD array can be described by

$$y = \frac{YL \cos \alpha}{h} \frac{1}{1 - (Y \sin \alpha)/h}$$

and

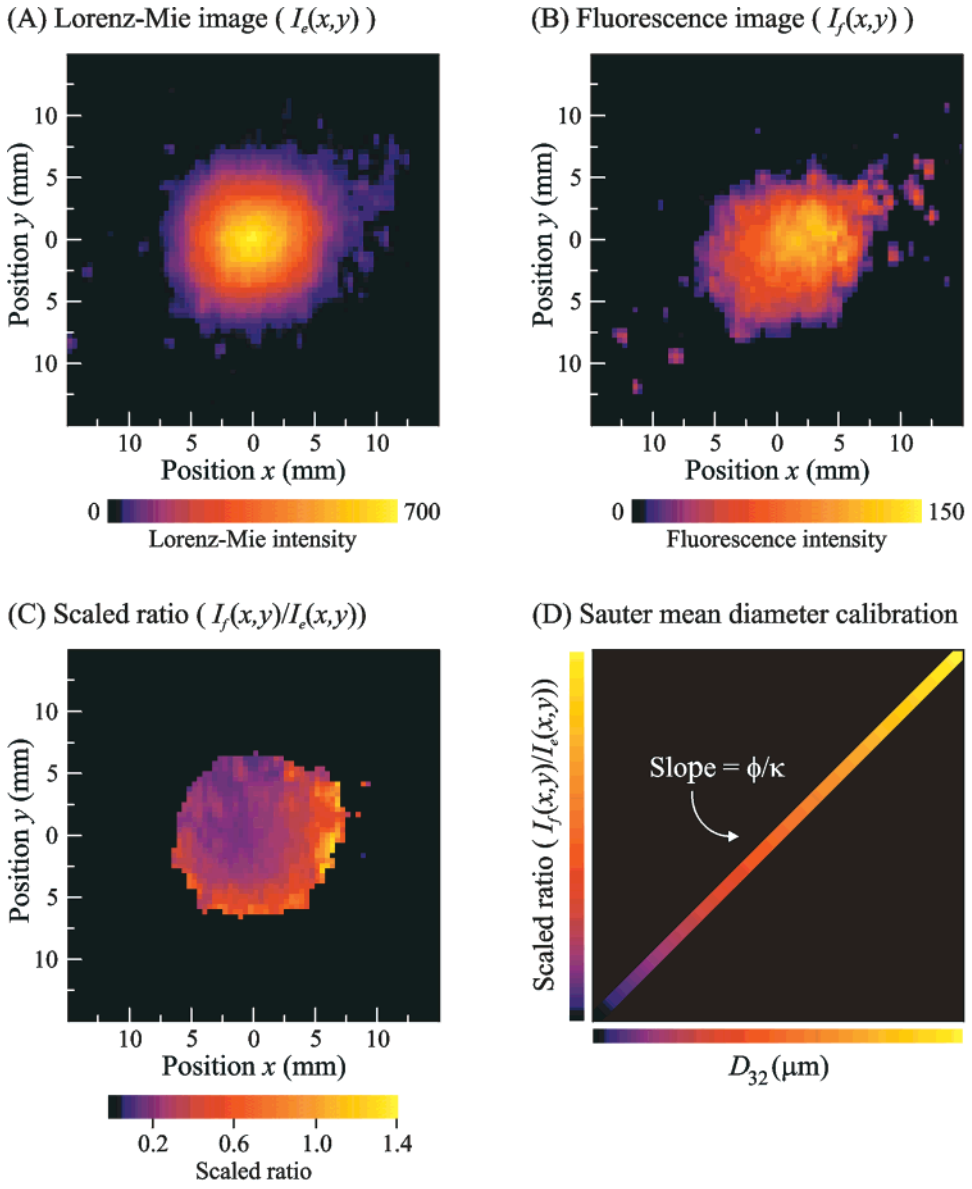

Figure 4. Comparison of the three image types obtained using optical patternation for the aerosol produced by a DIHEN at a position 30 mm from the tip of the nebulizer using an integration time of 5 ms/image. (A) Lorenz−Mie image of the planar elastic light scattering, (B) fluorescent image of the two-dimensional mass distribution, and (C) a spatial map of the Sauter mean diameter, D_{32}, (ratio image of B/A). The images were acquired for an oblique viewing angle of 32.5° subsequently corrected for perspective distortion. In all cases, the DIHEN was operated using a solution flow rate of 85 μL/min and a nebulizer gas flow rate of 0.25 L/min. (D) Illustration of the linearity of the scattering constants ϕ and κ used to calibrate the scaled ratio image for one of spatial Sauter mean droplet size distribution.

$$x = \frac{XL}{h}\frac{1}{1-(Y\sin\alpha)/h} \qquad (6)$$

where (x, y) are the coordinates of the perspective distorted image on the CCD array, (X, Y) are the coordinates of the actual image in the light sheet plane, α is the oblique viewing angle, L is the distance between the lens and the camera, and h is the distance from the center of the imaging lens to the scene center illuminated by the light sheet (Figure 3B).[58] In this work, the magnitude of α, Y, and h are 32.5°, 430 mm, and 800 mm, respectively. Thus, the term $Y \sin\alpha/h$ is smaller than 1 (for example, ~0.29 in the present studies). Accordingly, a MacLaurin binomial series expansion of the x, y eqs 6 can be performed:[58]

$$y = \frac{YL\cos\alpha}{h}\left(1+\frac{\sin\alpha}{h}Y+\frac{\sin^2\alpha}{h^2}Y^2+\frac{\sin^3\alpha}{h^3}Y^3+\ldots\right)$$

$$x = \frac{XL}{h}\left(1+\frac{\sin\alpha}{h}Y+\frac{\sin^2\alpha}{h^2}Y^2+\frac{\sin^3\alpha}{h^3}Y^3+\ldots\right) \qquad (7)$$

First-order approximation in the expanded x, y eqs 7 indicates that the image position on the CCD array varies inversely with h. When the camera is placed orthogonal to the light sheet (α = 0°), the first-order approximation is exact. At an oblique viewing angle, the first-order approximation introduces an error of relatively small magnitude (0−5% in intensity across an image ~300 mm in depth at oblique viewing angles of 60°−15°, respectively).[58]

Figure 4A−C illustrates the relation of three corrected images: scattering, fluorescence, and a scaled ratio of droplet size

(57) LSAP Program, Aerometrics/TSI Inc., St. Paul, MN 55164.

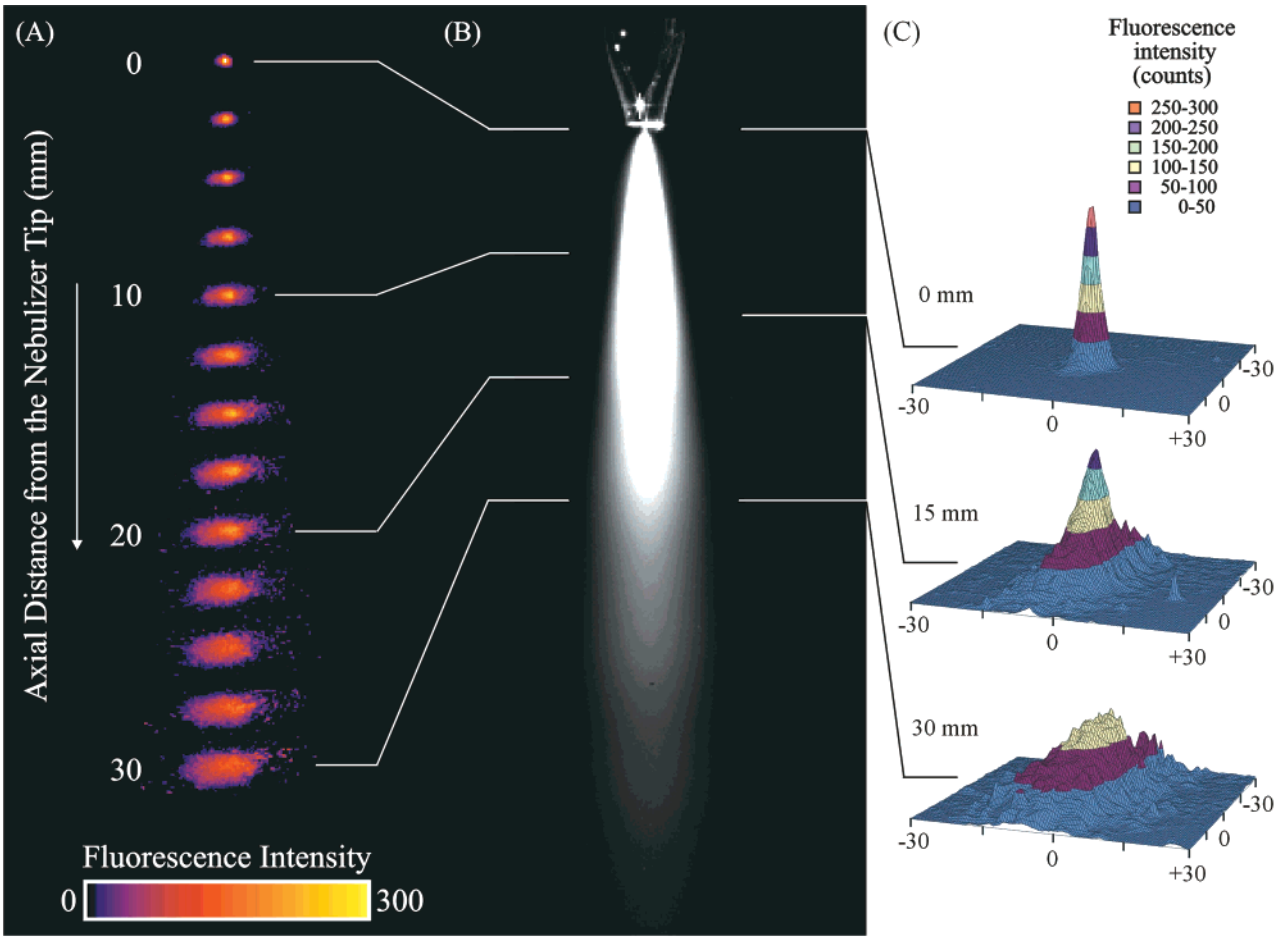

Figure 5. (A) Three-dimensional mass distribution obtained using the DIHEN at a solution flow rate of 85 μL/min and a nebulizer gas flow rate of 0.25 L/min. Images were collected using an oblique viewing angle of 32.5° and an integration time of 5 ms/slice. For quantitation, the images were corrected for perspective distortion. Subsequently, 30° of perspective was readded to each image for clarity. (B) Raw orthogonal-mode image to show the relative position of the spatial mass distributions shown in (A, C). (C) Three-dimensional plots of the droplet mass distribution shown for axial positions of 0, 15, and 30 mm from the nebulizer tip.

distribution. In calibrating the scaled ratio image to one of Sauter mean diameter (Figure 4D), the proportionality constants ϕ and κ are required, which are difficult to compute theoretically. These constants are also prone to systematic errors because they depend on many variables. Alternatively, an independent point-sizing technique such as PDPA can be used to empirically determine ϕ/κ at several points in the spray for interpolation of D_{32} from the scaled intensity ratio. For regions near the center of the spray, excellent agreement has been realized between D_{32} obtained with the optical patternator and the PDPA.[50,53] At the outer fringes of the spray, the patternator data provides a marginally larger distribution than the PDPA, which is attributed to the sampling methods of the two techniques. In low droplet number density regions, for instance at the fringes of the aerosol, the optical patternator is likely to register a more biased response for larger droplets because of the fixed exposure time and limited dynamic range of the CCD. On the other hand, the PDPA is a single-particle sizing technique which probes individual droplets for as long as required to reach a user defined number of droplets (e.g., 10 000).

(58) Lai, W.; Alfini, S.; Su, J. Development of an Optical Patternator for the Quantitative Characterization of Liquid Sprays. *10th International Symposium on Applications of Laser Techniques to Fluid Dynamics*, Lisbon, Portugal, July 10−13, 2000.

Three-Dimensional Mass Distributions. Figure 5 shows side-by-side illustrations of the raw image and an image stack representing a three-dimensional mass distribution of aerosol for the DIHEN probed using an oblique viewing angle of 32.5°. The images presented in Figure 5 were obtained by moving the aerosol perpendicular to the fixed light sheet position. Each image was acquired using an integration time of 5 ms/slice. Each slice was also corrected for oblique perspective distortion to perform the corrections of eq 5. To illustrate the three-dimensional mass distribution, 30° of perspective was subsequently added to each image. Fluorescence images were obtained at axial positions ranging from 0 to 30 mm from the tip of the nebulizer. Considering that the light sheet thickness was 2 mm, axial positions presented in Figure 5 represent the top position of the light sheet.

The maximum in mass distribution is observed close to the nebulizer tip where the sample aerosol is injected in to the ICP, for example, in ICPMS measurements.[3,45−47] Broader mass distributions are observed at larger axial distances from the nebulizer, which may result in aerosol loss when a spray chamber is used. This is a critical issue, especially when solution uptake rate is reduced.

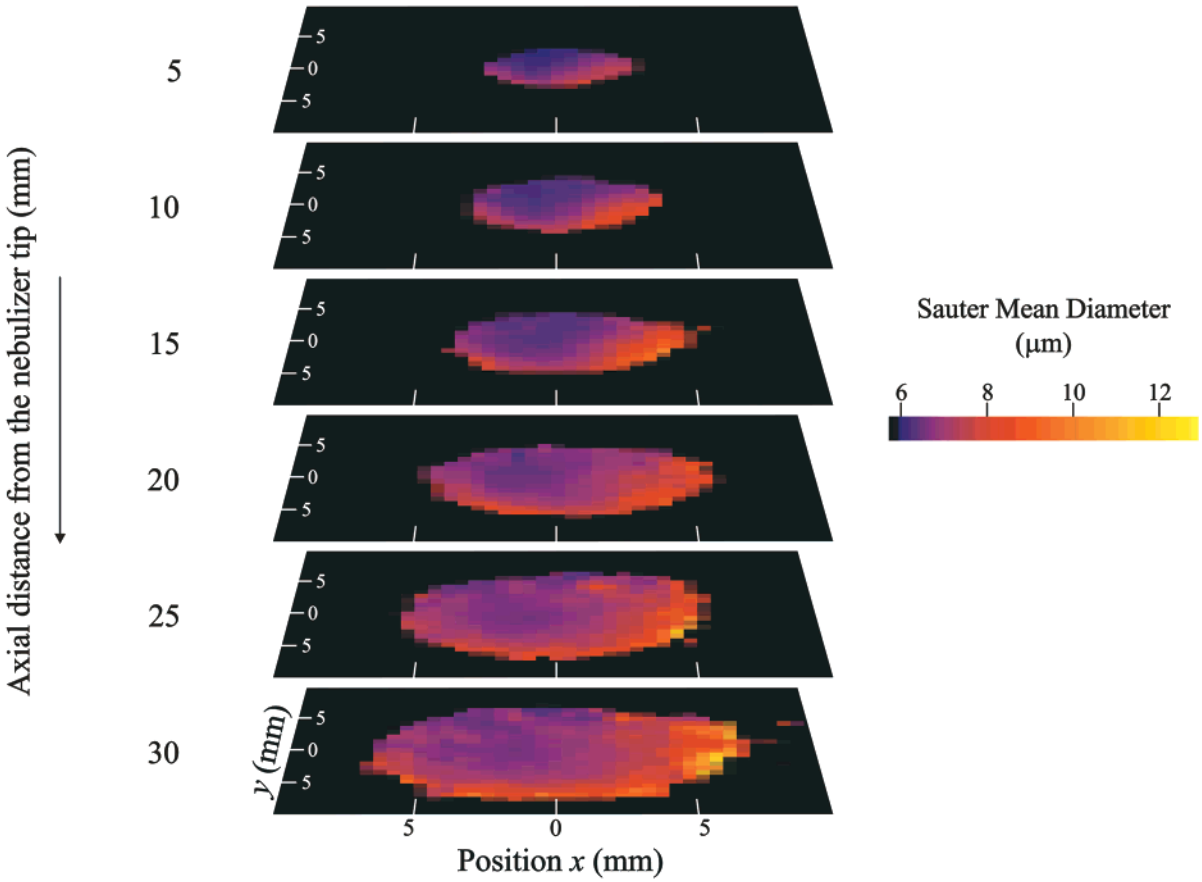

Figure 6. Three-dimensional droplet size distribution obtained using the DIHEN at a solution flow rate of 85 μL/min and a nebulizer gas flow rate of 0.25 L/min. Images were collected using an oblique viewing angle of 32.5° and an integration time of 5 ms/slice. For quantitation, the images were corrected for perspective distortion. Subsequently, 30° of perspective was readded to each image for clarity.

The peak in mass distribution begins in the center of the spray and is then moved slightly off-center at larger axial positions from the nebulizer tip (e.g., 20 mm). Previous reports using a PDPA have shown that concentric pneumatic nebulizers show decreasing volume flux (or mass flux) away from the center of the aerosol.[54] While light sheet attenuation across the aerosol can contribute to off-center peaks in intensity, the light sheet in Figure 5 initially interacts with the aerosol from the left side of the image. If light sheet attenuation was high, then the fluorescence peak intensity would be biased to the left side of the image, which is opposite of what is observed. Small variations in the gas dynamics at the tip of the nebulizer may contribute to slightly variable mass distributions for all pneumatic nebulizers.

At larger axial positions away from the nebulizer tip (e.g., 30 mm), the images show local points of low fluorescent intensity. This is likely attributed to individual large droplets encountered in the fringes of the spray (see below). Because the integration time for each image is only 5 ms and droplet velocity decreases at farther distances from the tip of the nebulizer, these local points show individual droplets that possess longer residence times in the 2-mm-thick light sheet. The sensitivity limits in optical patternation are controlled by sources such as the laser fluence, image integration period, and particle size, which clearly depend on the experimental arrangement and requirements of the analytical task.

Three-Dimensional Droplet Size Distributions. Figure 6 shows the three-dimensional droplet size distribution for the DIHEN aerosol at axial positions of 5−30 mm from the tip of the nebulizer. These images are first corrected for perspective distortion before dividing the fluorescent images by the corresponding Lorenz−Mie elastic light-scattering images. To stack the images, 30° of perspective angle is subsequently added to each image using the graphics software described above. The scaled intensity ratio image is converted to droplet size distribution by evaluating the proportionality constants ϕ and κ empirically using a PDPA as described above.

Two important observations are made from the data in Figure 6. First, similar to previous studies,[41,42,54,59] larger droplets are found along the fringes of the aerosol cone. Second, droplet diameters appear to increase across the particle field at larger axial positions (e.g., 30 mm). At large axial positions, solvent evaporation and droplet coagulation contribute to larger droplet sizes and distributions. Interaction of these larger droplets with the eddy current region of the ICP can result in increased noise, impairing precision in analytical measurements.

In addition to the image corrections described above, two additional categories of potential systematic image distortion may arise. The light sheet and the scattered radiation can be attenuated in the aerosol interrogation region and from this region to the CCD. Both of these sources of attenuation can be serious in dense

(59) Dodge, L. G.; Rhodes, D. J.; Reitz, R. D. *Appl. Opt.* **1987**, *26*, 2144−2154.

sprays.[60] The second source of error is primarily concerned with fluorescence effects. For example, the fluorescence signal from the vapor phase may overexpose certain regions of the image. Regions of high vapor pressure, such as the interior of the spray, may be over exposed relative to the fringe region where air entrainment and diffusion of the vapor away from the aerosol is more efficient. Additionally, in nonsymmetrical spray environments, nonuniform vaporization can convolute the fluorescent image. Temperature-dependent absorption and oxygen quenching of the fluorescent species may also occur, but the latter perhaps can be compensated by operating in the saturated fluorescence regime. In general, the magnitude of these errors depends on the experimental arrangement. However, droplet size data reported thus far with the PDPA technique and the optical patternator approaches have correlated well.[48,53] Thus, the above potential sources of error were neglected in this preliminary work.

In reference to droplet size calibration (Figure 4D), two issues are of interest. First, what is the ultimate calibration standard for optical patternation? Second, would measurements with a monodisperse calibration aerosol be possible? Two potential calibration strategies are to implant uniform size microspheres into a transparent bar or to measure monodisperse aerosols produced by the vibrating orifice or the MDMI. Such strategies should eliminate the need for independent particle-sizing techniques, such as PDPA, for D_{32} image calibration.

CONCLUSIONS

The optical patternator technique was used to quickly obtain spatially resolved spray structures, mass distributions, and droplet size distributions from the aerosol produced by a direct injection high efficiency nebulizer. In principle, the optical patternator technique can be extended to provide three-dimensional droplet velocity and droplet temperature distributions. Droplet velocities can be measured, similar to particle-imaging velocimetry, by recording two successive images of the droplet field over a known time interval and using autocorrelation or cross-correlation techniques. Spatially resolved droplet temperature distributions can be explored by using a pulsed laser and measuring droplet fluorescence decay rates and/or the rainbow angle, both of which are temperature dependent.[3,61] Depending on the particular experimental arrangement, optical patternation can be applied to the investigation of transient spray processes down to the nanosecond time scale to yield a better understanding of fundamental processes prevalent in analytical spectroscopies. The investigation of transient processes can reveal temporal structural changes in the aerosol or can be used in the analysis of modulated spray systems.[49,53,60] Work in these areas is in progress in our laboratories.

ACKNOWLEDGMENT

The research was sponsored by grants from the U.S. Department of Energy (DE-FG02-93ER14320), the National Science Foundation (CHE-9505726 and CHE-9512441), and J. E .Meinhard Associates, Inc. Scholarship support for J.A.M. was provided by the ARCS Foundation and an ACS Division of Analytical Chemistry Fellowship sponsored by Glaxo Wellcome. We thank Dave Scott (Upper Arlington, OH) for valuable discussions on image processing and Roger Rudoff (Aerometrics Inc., Sunnyvale, CA) for his assistance in facilitating this work.

Received for review February 25, 2000. Accepted June 11, 2000.

AC000239Y

(60) Su, J.; Drake, M. C.; Fansler, T. D.; Harrington, D. L. Towards Quantitative Characterization of Transient Fuel Sprays Using Planar Laser Induced Fluorescence Imaging. *11th Annual Conference on Liquid Atomization and Spray Systems*, Sacramento, CA, May 19−22, 1998.

(61) Sankar, S. V.; Ibrahim, K. M.; Buermann, D. H.; Fidrich, M. J.; Bachalo, W. D. An Integrated Phase Doppler/Rainbow Refractometer System for Simultaneous Measurement of Droplet Size, Velocity, and Refractive Index. *3rd International Conference on Optical Particle Sizing*, Yokohama, Japan, August 23−26, 1993.

(62) Minnich, M. G.; McLean, J. A.; Montaser, A. Spatial Aerosol Characteristics of a Direct Injection High Efficiency Nebulizer via Optical Patternation. Submitted to *Anal. Chem*.